Experimental validation of a vanadium redox flow battery model for state of charge and state of health estimation

Alejandro Clemente[1*], Manuel Montiel[2,3], Félix Barreras[2], Antonio Lozano[2] and Ramon Costa-Castelló[4]

*Corresponding author: alejandro.clemente.leon@upc.edu

[1] Institut de Robòtica i Informàtica Industrial, CSIC-UPC, Llorens i Artigues 4-6, 08028 Barcelona, Spain.

[2] Instituto de Carboquímica, CSIC, Miguel Luesma Castán, 4, 50018 Zaragoza, Spain.

[3] Fundación ARAID, Avda de Ranillas, 1-D, 50018, Zaragoza, Spain.

[4] Universitat Politècnica de Catalunya, Avinguda Diagonal, 647, 08028 Barcelona, Spain.

Abstract This study presents a vanadium redox flow battery model that considers the most important variables that have a crucial role in the performance of the system. A complete model divided in an electrochemical, thermal, hydraulic and voltage submodels is presented. The analytic analysis of the model is carried out to reduce the system order according to some conservation laws. Based on this analysis, a subsequent calibration of the model parameters is developed using real experimental data. The validation is performed comparing the real measured voltage and the one estimated with the model. To calibrate the model an algorithm based on the implementation of a particle swarm optimizer is used. Results obtained in both short and long-term operation are presented, in order to compare and validate if the model can be used for both state of charge and state of health estimation.

Keywords: Redox flow battery, Nonlinear model, State of Charge, State of Health, Particle Swarm Optimization

1 INTRODUCTION

Among all types of energy storage systems (ESS), vanadium redox flow batteries (VRFB) stand out for their high efficiency (70-90%), long life cycle, safety and the possibility to decouple both energy and power sizes [4].

One of the main challenges in the study and analysis of a VRFB consists on the correct caracterization of its behaviour through mathematical models. The importance of developing mathematical models for VRFB is reflected in the literature [5] [17], where it is possible to find one of the most accepted electrochemical models developed by Skyllas-Kazacos, who pioneered the use of vanadium in redox flow batteries [19].

Models can be classified as static or dynamic, depending on whether the effect of time is taken into account, and as distributed or lumped parameter models, depending on the space dimension. Tools such as COMSOL are used to analyze and develop distributed models. However, for control purposes, distributed models are not used due to its complexity, relevant computational cost, resources and time [3]. In counterpart, vast majority of works concerning VRFB control problems, use lumped parameters models.

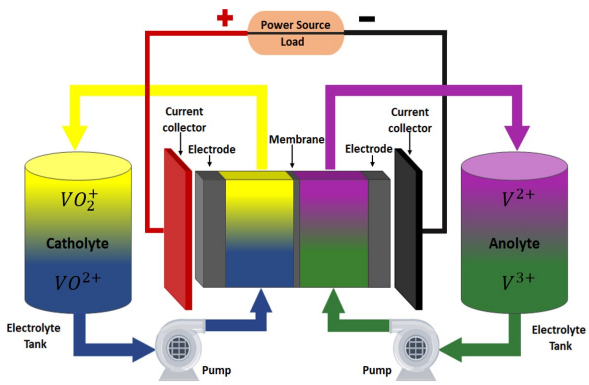

Figure 1: Vanadium redox flow battery scheme with its main components.

Most of these lumped parameter models use different hypothesis and assumptions that simplify their complexity. Although a vast majority of these assumptions may not be entirely realistic, they help in the understanding, formulation and analysis of the model. This is the case of the mentioned Skyllas-Kazacos electrochemical models, where the same flow rate is considered in both parts of the system, same species concen-

tration inside the cell and tanks, as well as a constant temperature to estimate the open circuit voltage (OCV) by the Nernst equation.

In general, most of the works found in the literature related to VRFB modeling, study and analyze the behaviour of different variables as the evolution of the species concentration, voltage, temperature, pressure, state of charge (SOC) or state of health (SOH). The evolution of species concentrations can be found in lot of studies, from lesser to greater complexity. Thus, Skyllas-Kazacos presents in [18] a model that expresses the dynamics of the vanadium species considering the different ion transport mechanisms such as diffusion, migration and convection. This model has been improved in some works introducing the effect of other phenomena, such as the oxidation of vanadium V^{2+} due to the presence of air inside the negolyte tank [11]. These models only consider the participation of vanadium species. However, there are other species that can be considered such as the water and hydrogen ions. The inclusion of these species not only improves the better understanding of the electrochemical part, but also allows to consider other important effects, such as the Donnan potential in the computation of the voltage [10]. The dynamics of the water crossover phenomena are analyzed in [15], while those of the hydrogen ions have also been studied [16].

Regarding voltage computation, most of the works are focused on the determination and analysis of the different overpotentials and phenomena that affect its computation. The OCV is discussed in [7], showing the discrepancy between the common models and experimental data, presenting a complete form of the Nernst equation considering the proton activity and Donnan potential. Other works such as [9] and [13] are focused on the computation of the concentration and activation overpotentials.

With respect to the thermal model, different works presented in the literature study the temperature dynamics in some parts of the system, those inside the cell being specially interesting. Thus, a thermal model is shown in [24], that allows to compute the temperature inside the cell taking into account the temperature in the pipes and tanks. The inclusion of the dynamics due to self-discharge reactions is presented in [20] while the analysis of the shunt current effect is investigated in [23].

Pressure is another important variable to take into account that is directly related to the flow rates of the system, which have an important role in control purposes such as optimal control. Therefore, some studies analyze the behaviour of the pressure inside a VRFB system as can be observed in [22].

Among all variables of interest regarding the performance of a VRFB, state of charge (SOC) and state of health (SOH) stand out as the most important. There exist different definitions for these variables, according to the parameters and variables that are considered for their computation [14]. However, the vast majority of these definitions present the SOC and SOH as a function of the species concentrations, which makes it necessary to choose an appropriate electrochemical model [6].

Usually, most of the studies that present an electrochemical model for SOC and SOH computation are only validated theoretically or by means of simulations. However, experimental validation is usually limited to the estimation of one of these variables, and under some assumptions that can differ from a real battery behaviour. Moreover, for this cases, it is more difficult to find studies that present a general model that comprises the most important variables described in a single model.

Thus, in this work, a complete model that considers the most important effects of a VRFB is presented. The model can be divided into four submodels, according to the most important variables, which are: electrochemical, voltage, thermal and hydraulic ones. The main objective of this work is to understand the dynamics of each one of these subsystems in an efficient way, presenting the main equations that describe the different effects, and relate them with the other submodels. With these dynamics, the most important performance indicators such as the SOC, SOH, capacity and efficiencies are defined. A general model that can deal with short and long term scenarios is presented in order to see if it is suitable for SOC and SOH. In order to validate the model, an experimental setup has been developed to estimate these two parameters calibrating the model with voltage and current measurements obtained from different experiments in short and long term campaigns. In order to calibrate the model, there exist different algorithms and methods that can be used, being the particle swarm optimization (PSO) a good choice to estimate a certain number of parameters whose value is only known within a particular range [26]. Using the PSO technique it is possible to calibrate the model using experimental data extracted from a VRFB that has been designed, consisting on a cell with two little tanks, presenting a similar aspect to the VRFB scheme shown in Figure 1.

The paper is organized as follows. Section 2 presents the formulated model, while in Section 3, a conservation study is developed in order to see if the mass and charge conservation principles are fulfilled for the model dynamics presented. Section 4 presents the experimental validation of the model, describing the experimental setup and the different results obtained from the model calibrated using the PSO algorithm. Finally, Section 5 presents the main conclusions.

2 MODEL FORMULATION

The model can be formulated in different submodels according to the properties and characteristics of the state variables. The four submodels into which the general model has been divided are the electrochemical, the thermal, the hydraulic and the voltage ones. All submodels interact with the others, sharing some parameters and variables to define the most important performance indicators, typical of any energy storage system.

2.1 Electrochemical model

Among the different electrochemical models that exist for VRFB, the dynamic model proposed by Skyllas-Kazacos is the most widely used and accepted [18]. Based on this model, it is possible to express the behaviour of the vanadium species inside the system, considering the most important phenomena such as the redox reactions and the ion transport due to ion crossover methods.

On the one hand, the redox reactions that take place inside the cell/stack of a VRFB are:

$$V^{2+} \rightleftarrows V^{3+} + e^- \tag{1}$$

$$VO_2^+ + 2H^+ + e^- \rightleftarrows VO^{2+} + H_2O\ , \tag{2}$$

where V^{2+} and V^{3+} are the vanadium species in the negative side (1), and VO^{2+} and VO_2^+ are the vanadium species in the positive side (2), which are commonly expressed by the oxidation state as V^{4+} and V^{5+}, respectively.

On the other hand, the ion crossover methods appear due to the self-discharge reactions that occur on both sides of the system. The mass balance due to these reactions in both positive and negative electrodes can be described separately. On the one hand, in the negative electrode the self-discharge reactions occurs due to the presence of VO^{2+} and VO_2^+ that have moved across the membrane. These species are reduced by V^{2+} to become V^{3+}:

$$VO^{2+} + V^{2+} + 2H^+ \longrightarrow 2V^{3+} + H_2O \tag{3}$$

$$VO_2^+ + 2V^{2+} + 4H^+ \longrightarrow 3V^{3+} + 2H_2O \tag{4}$$

$$VO_2^+ + V^{3+} \longrightarrow 2VO^{2+}\ . \tag{5}$$

On the other hand, the same behaviour occurs in the positive electrode, where vanadium species V^{2+} and V^{3+} cross the membrane and are oxidized by VO_2^+ to VO^{2+}:

$$V^{2+} + 2VO_2^+ + 2H^+ \longrightarrow 3VO^{2+} + H_2O \tag{6}$$

$$V^{3+} + VO_2^+ \longrightarrow 2VO^{2+} \tag{7}$$

$$V^{2+} + VO^{2+} + 2H^+ \longrightarrow 2V^{3+} + H_2O\ . \tag{8}$$

Skyllas-Kazacos considers several assumptions that are the following [1]:

- Electrolytes are perfectly mixed.
- The total number of moles of the species remains constant.
- Vanadium concentrations are uniformly distributed in the cell and tanks, without considering the hydrogen ions and water.
- Electrolyte flow rate is the same in both half-cells.
- Electrolyte temperature remains constant.
- Self-discharge reactions occurs instantaneously by ion crossover.
- Vanadium and hydrogen ions are transported through the membrane by diffusion. Other transport mechanisms of water and ions such as migration, convection or osmosis are neglected.
- Diffusion coefficients are constant.
- Gas evolution or other side reactions during charging/discharging neglected.

Considering the above assumptions, the general expression that describes the concentration evolution of the species is:

$$\varepsilon v^e \frac{\partial c_i^c}{\partial t} = q \cdot (c_i^t - c_i^c) \pm s^e \frac{j}{F} + d_i\ , \tag{9}$$

where ε is the electrode porosity, v^e is the electrode volume and c_i^c is the concentration of vanadium species i inside the cell, expressed in mol·m^{-3}.

The electrode volume v^e depends only on the dimensions of the electrode and the number of equal cells of the stack:

$$v^e = N \cdot h^e \cdot w^e \cdot l^e\ , \tag{10}$$

N being the number of cells, and h^e, w^e and l^e the height, thickness and length, respectively, in m. These dimensions have been defined in this work considering the orientation shown in Figure 2.

As can be noticed, the cell concentration expression (9) can be splitted in three parts. The first term defines the change of species due to the inlet and outlet flux of electrolyte, generated by the electrolyte flow rate q in m^3· s^{-1}. The second term implies the role of the redox reactions (1) - (2) due to the presence of the electrons generated for the existing current between the collectors. This effect represents the current flux perpendicular to the cell, and is described by a current density j, expressed in A·m^{-2}, F that is the Faraday constant (96845.33 C·mol^{-1}) and the electrode surface s^e which depends on the electrode height and length:

$$s^e = h^e \cdot l^e\ . \tag{11}$$

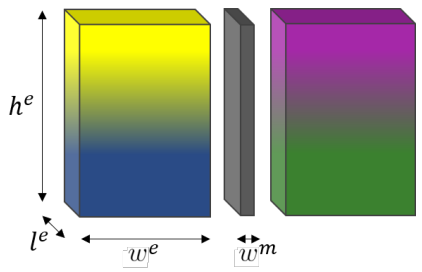

Figure 2: 3D Scheme of a single cell composed by two electrodes and a membrane. h^e: electrode and membrane height, l^e: electrode and membrane length, w^e: electrode thickness, w^m: membrane thickness.

Finally, last term d_i is the total flux of species i across the membrane, which is the ion crossover effect and, in this work, it is only associated with the diffusion. The diffusion phenomenon occurs because the membranes allow the crossover of vanadium species from one side of the cell to the other. This movement from high to low concentration areas is driven by concentration gradients, and therefore depends on each vanadium species, modelled to obey Fick's law:

$$d_i = \frac{s^m}{w^m} \cdot (\alpha_{2_i} k_2 c_2^c + \alpha_{3_i} k_3 c_3^c + \alpha_{4_i} k_4 c_4^c + \alpha_{5_i} k_5 c_5^c) \,, \quad (12)$$

where s^m is the membrane surface in contact with the electrolyte, which according to Figure 2 can be computed as s^e, α_{k_i} is the mass balance between the particular vanadium species i with the other species k, and k_i is the diffusion coefficient of each vanadium species, expressed in $\mathrm{m}^2 \cdot \mathrm{s}^{-1}$.

In most of the studies, the diffusion coefficients k_i are assumed to be constant and invariant. However in this work a variable obeying the Arrhenius equation have been considered [21]:

$$k_i = A_i e^{\frac{-E_a}{RT^c}} \,, \quad (13)$$

A_i being the pre-factor, which is a constant that depends on the membrane material and is different for each vanadium specie, E_a the activation energy of the vanadium species (17340 $\mathrm{J \cdot mol^{-1}}$), which is assumed to be the same for all species [27], R is the universal gas constant (8.314 $\mathrm{J \cdot mol^{-1} \cdot K^{-1}}$) and T^c is the electrolyte temperature inside the cell/stack. Therefore, each species has a different pre-factor that depends on the membrane composition.

For the tank dynamics, as they are isolated parts of the system whose only function is to store the electrolyte, the only important term is the inlet and outlet flux of electrolyte:

$$v^t \frac{\partial c_i^t}{\partial t} = q \cdot (c_i^c - c_i^t) \,, \quad (14)$$

where v^t is the elecrolyte volume inside the tank and c_i^t is the concentration of species in the tank, sharing the same units of $\mathrm{mol \cdot m^{-3}}$ as the cell concentration. As there is not any flux of current going through the tanks, and species cannot escape from them, the second and third terms of (9) are neglected.

Considering the cell and tank dynamic expressions formulated by (9) and (14), some modifications have been made respect to the model presented by Skyllas-Kazacos [18] in order to make it more realistic. They are:

- Electrolyte flow rate can be different in both half-cells. Thus, a clear distinction between the electrolyte circuits is made, distinguishing the negative (-) from the positive (+) side.
- Electrolyte temperature varies and it is computed by a thermal model closely related to the electrochemical one.
- Hydrogen ions and water are considered. They are usually neglected, but have an important role in the system operation.

As this work pretends to be a tool for the understanding and developing of a possible model, the vanadium, water and hydrogen ion models are presented separately. All of them are formulated in the state space domain to facilitate the understanding and comparison.

2.1.1 Vanadium electrochemical model

Considering expressions (9) and (14), the vanadium electrochemical model can be formulated in the state space notation as:

$$\dot{\boldsymbol{x}} = \mathbf{A}\boldsymbol{x} + \mathbf{B}_{-}\boldsymbol{x} \cdot q_{-} + \mathbf{B}_{+}\boldsymbol{x} \cdot q_{+} + \mathbf{b} \cdot j \,, \quad (15)$$

where q_{-} and q_{+} are the flow rates of negolyte and posolyte, j is the current density and the state vector, $\boldsymbol{x}$, is defined as $\boldsymbol{x}=[c_2^c \;\; c_3^c \;\; c_4^c \;\; c_5^c \;\; c_2^t \;\; c_3^t \;\; c_4^t \;\; c_5^t]^\top$; where c_i^p stands for the concentration of vanadium species i in space p, with $p = \{c, t\}$ meaning cell and tank, respectively. Matrix $\mathbf{A}$ is directly related to the diffusion d_i, matrices $\mathbf{B}_{-}$ and $\mathbf{B}_{+}$ with the flow rates effect and vector $\mathbf{b}$ is related to the presence of electrons due to the redox reaction. All matrices and vectors appear summarized in the Appendix section.

Using this formulation, j, q_{-} and q_{+} are the input variables which are assumed to be known, being easily measured and controlled.

2.1.2 Hydrogen electrochemical model

The same procedure can be developed for the hydrogen ions model. In that case, it can be represented as:

$$\dot{\boldsymbol{x}}_{\mathbf{H}} = \mathbf{A}_{\mathbf{H}}\boldsymbol{x}_{\mathbf{H}} + \mathbf{B}_{\mathbf{H}_{-}}\boldsymbol{x}_{\mathbf{H}} \cdot q_{-} + \mathbf{B}_{\mathbf{H}_{+}}\boldsymbol{x}_{\mathbf{H}} \cdot q_{+} + \mathbf{B}_{\mathbf{d_s}}\boldsymbol{x} + \mathbf{b}_{\mathbf{H}} \cdot j \,, \quad (16)$$

where $\boldsymbol{x}_{\mathbf{H}}$ is the new state vector of proton concentrations considering the cell and tanks and is defined as $\boldsymbol{x}_{\mathbf{H}} = [c^c_{H^+_-} \quad c^c_{H^+_+} \quad c^t_{H^+_-} \quad c^t_{H^+_+}]^\top$. Matrix $\mathbf{A_H}$ expresses the diffusion due to the concentration difference of both sides. Matrices $\mathbf{B}_{\mathbf{H}_+}$ and $\mathbf{B}_{\mathbf{H}_-}$ are related to the inlet and outlet fluxes from cell and tanks and matrix $\mathbf{B}_{\mathbf{d}_s}$ is related to the proton diffusion due to the self-discharge reactions, which is related to the vanadium species $\boldsymbol{x}$. Finally, vector $\mathbf{b_H}$ expresses the variation of protons due to the charging/discharging current density j where, according to the redox reactions (1) - (2), it is possible to see how in the negative part, the protons do not appear, while in the positive one, the redox reaction involves 2 hydrogen ions H^+ for each electron e^-.

2.1.3 Water electrochemical model

Another important species to consider is the water. In this case, the electrochemical expressions that describe its evolution inside the system can be formulated in state space as:

$$\dot{\boldsymbol{x}}_{\mathbf{H_2O}} = \mathbf{A}_{\mathbf{H_2O}}\boldsymbol{x} + \mathbf{B}_{\mathbf{H_2O}_-}\boldsymbol{x}_{\mathbf{H_2O}} \cdot q_- + \mathbf{B}_{\mathbf{H_2O}_+}\boldsymbol{x}_{\mathbf{H_2O}} \cdot q_+ + \mathbf{b}_{\mathbf{H_2O}} \cdot j \,, \tag{17}$$

where $\boldsymbol{x}_{\mathbf{H_2O}}$ is the state vector of water concentrations considering the cell and tanks, and it is defined as $\boldsymbol{x}_{\mathbf{H_2O}} = [c^c_{H_2O_-} \quad c^c_{H_2O_+} \quad c^t_{H_2O_-} \quad c^t_{H_2O_+}]^\top$. The matrix $\mathbf{A}_{\mathbf{H_2O}}$ contains the diffusion coefficients of the vanadium species and is related to the self-discharge diffusion. Matrices $\mathbf{B}_{\mathbf{H_2O}_-}$ and $\mathbf{B}_{\mathbf{H_2O}_+}$ are related to the inlet and outlet fluxes and are exactly equal to the protons matrices, and vector $\mathbf{b}_{\mathbf{H_2O}}$ is related to the variation of water in the positive part due to the current density.

2.2 Performance parameters

Among the many parameters that can be established depending on the variable or characteristic to be analyzed, it is worth highlighting some of them that are commonly studied and used for any type of ESS. These main indicators are the SOC and SOH.

2.2.1 State of charge

The state of charge is one of the most common indicators of a battery, that is used to denote the capacity that is currently available. It is directly related to the amount of species inside the global system. In particular, the SOC of a VRFB is computed as the ratio of active species V^{2+} and VO_2^+ with respect to the total concentration of species in each side. Thus, it should be noted that there exist two different SOC, defined as (SOC_-) and (SOC_+) to represent the SOC in the negolyte and posolyte, respectively.

As the volume of the tanks is generally much greater than that of the cell/stack, the role of the cell concentration is neglected to calculate the SOC in most studies. Moreover, many of them assume that the concentrations on both sides of the system are the same and evolve equally with time, concluding that there exist only one definition of SOC, being exactly the same for both parts:

$$\mathrm{SOC} = \frac{c_2}{c_2 + c_3} = \frac{c_5}{c_4 + c_5} \,. \tag{18}$$

Although these assumptions allow to simplify the VRFB model, they have not been considered since the purpose of this study is to develop a complete and realistic model that includes the main operating phenomena, as well as degradation. Therefore, considering the effect of the species transport mechanism, it is essential to differentiate between negolyte and posolyte concentrations, obtaining the following expressions:

$$\mathrm{SOC}_- = \frac{c_2}{c_2 + c_3} \tag{19}$$

$$\mathrm{SOC}_+ = \frac{c_5}{c_4 + c_5} \,. \tag{20}$$

Furthermore, considering the role of the cell concentration, that has influence on the system voltage and may be different from that of the tanks, expressions (19) and (20) must be reformulated as:

$$\mathrm{SOC}_- = \frac{c^t_2 v^t_- + c^c_2 v^c}{c^t_2 v^t_- + c^c_2 v^c + c^t_3 v^t_- + c^c_3 v^c} \tag{21}$$

$$\mathrm{SOC}_+ = \frac{c^t_5 v^t_+ + c^c_5 v^c}{c^t_4 v^t_+ + c^c_4 v^c + c^t_5 v^t_+ + c^c_5 v^c} \,. \tag{22}$$

As can be noticed from (21) and (22), the SOC has been recomputed as a ratio of mass species, taking into account the volumes of the cell and tanks. This expression is more realistic and considers all vanadium species concentrations along the system.

However, it is important to note that the total amount of energy accumulated in the system will be given by the electrolyte with less SOC, in order to restrict the maximum energy that can be extracted. Accordingly, the correct expression of the SOC must be defined as:

$$\mathrm{SOC} = min\left(\mathrm{SOC}_-, \mathrm{SOC}_+\right) . \tag{23}$$

2.2.2 State of health

The state of health can be computed as the ratio between the amount of mass available in a certain moment with respect to the original one. In this case, the SOH has not been extensively analyzed in the literature, since, as has been commented, many of the studies do not consider the mass transport mechanisms. Nevertheless, it is one of the most important parameters since it is relevant for the life cycle of a battery.

For the VRFB, following with the definition presented for the SOC in (23), the SOH can be computed as the minimum amount of moles available between the two parts of the system, with respect to the ideal one:

$$\mathrm{SOH} = \frac{min\,(m_-, m_+)}{m^*}\,, \tag{24}$$

where m_- and m_+ define, respectively, the total number of moles, in the negolyte and posolyte parts, which can be computed by means of the following expressions:

$$m_- = v^c \cdot c_-^c + v_-^t \cdot c_-^t \tag{25}$$

$$m_+ = v^c \cdot c_+^c + v_+^t \cdot c_+^t\,, \tag{26}$$

c_- being the sum of V^{2+} and V^{3+} species concentrations corresponding to the negolyte and c_+ the sum of VO^{2+} and VO_2^+ for the posolyte part.

The other variable of (24) is the ideal mole distribution m^*, which can be defined from the total number of vanadium moles of the system as:

$$m^* = \frac{m}{2}\,, \tag{27}$$

where m denotes the vanadium moles of the system, which can be computed as the sum between both parts:

$$m = m_- + m_+ \tag{28}$$

2.3 Thermal model

Following the principle of conservation of energy, a dynamic thermal model can be formulated based on energy balance equations for the different parts of the system. Thus, temperature inside both tanks, cell and pipes can be considered. Regarding the heat generated from the pumps, it is convenient to differentiate between the temperature inside the pipes in two different parts, as depicted in Figure 3.

Among different thermal dynamic models for VRFB based on conservation of energy that appear in the literature, Tang et al. presents a model that considers the temperatures displayed in Figure 3, and takes into account the effect of pump heat and the self-discharge reactions due to the ion crossover mechanisms [24]. However, despite being a fairly realistic model, different assumptions have been taken into account:

- Temperature is uniformly distributed in each part of the system.
- Heat is transferred in each part between the electrolyte and the surrounding air.
- Cell heat is generated by the cell resistance and electrochemical and self-discharge reactions.

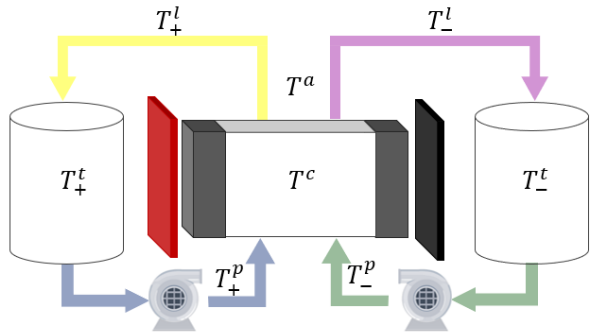

Figure 3: Temperature measurements in the different parts of the system. T_+^t: posolyte tank, T_+^l: posolyte line, T_+^p: posolyte pump line, T_-^t: negolyte tank, T_-^l: negolyte line, T_-^p: negolyte pump line, T^c: cell and T^a: air temperature.

One of the novelties of this work is the introduction of the heat generated due to the chemical reactions, considering their entropy. This new consideration adds more reality to some of the accepted thermal models presented in different works [25].

Similarly to the electrochemical model, the temperature inside each part T_i, changes according to the inlet and outlet flux of electrolyte with the contiguous part T_o. This change of temperature can be formulated as:

$$v c_p \rho \frac{\partial T_i}{\partial t} = q_k c_p \rho \cdot (T_o - T_i)\,, \tag{29}$$

where q_k is the electrolyte flow rate in the posolyte and negolyte sides, expressed in $m^3 \cdot s^{-1}$, c_p is the specific heat capacity of the electrolye in $J{\cdot}kg^{-1}{\cdot}K^{-1}$ and ρ is the electrolyte density expressed in $kg{\cdot}m^{-3}$.

Considering (29) and the previous assumptions, it is possible to express the temperature inside the cell T^c as:

$$\begin{aligned} 2v^c c_p \rho \frac{\partial T^c}{\partial t} &= q_+ c_p \rho \cdot (T_+^p - T^c) + q_- c_p \rho \cdot (T_-^p - T^c) \\ &+ u^c s^c \cdot (T^a - T^c) + (s^e j)^2 r \\ &+ s^e \frac{j}{F} \cdot (\Delta S_+ - \Delta S_-) T^c + d_T\,, \end{aligned} \tag{30}$$

where T_+^p and T_-^p are the temperatures at the pump outlet in the positive and negative sides, respectively in K, u^c is the overall heat transfer coefficient of the cell in $W{\cdot}m^{-2}{\cdot}\,K^{-1}$, s^c is the cell surface in m^2, T^a is the surrounding air temperature and r is the cell resistance in Ω. The first and second terms represent the change of temperature according to (29) for the positive and negative parts, respectively. The third term is related to the heat transferred between the cell surface and the surrounding air. The fourth term defines the heat generated inside the cell in form of Ohmic losses due to the

Joule effect. Fifth term represents the change of temperature due to entropy. Finally, d_T defines the changes of temperature due to the self-discharge reactions. This last term is related to the changes of enthalpy ΔH of the different reactions and can be modeled as:

$$d_T = \frac{s^m}{w^m}[k_2 c_2^c \cdot (-\Delta H_{(3)}) + k_3 c_3^c \cdot (-\Delta H_{(4)}) + k_4 c_4^c \cdot (-\Delta H_{(6)}) + k_5 c_5^c \cdot (-\Delta H_{(7)})] \,, \tag{31}$$

where $\Delta H_{(i)}$ is the change of enthalpy for the self-discharge reactions. The enthalpies of the different species are constant and can be found in the literature. Considering their values it is possible to obtain the change of enthalpy of the self-discharge reactions (3 - 4) and (6 - 7). Table 1 presents the value of the species and self-discharge reactions enthalpies.

Once the cell temperature evolution has been clarified, it is possible to develop the same analysis for the other parts of the system. It is important to notice that the expressions for the negative and positive part of the system are equal, due to the fact that can be seen as symmetrical with respect to the cell. In the vast majority of studies, they are considered equal, because they can be seen as symmetrical, assuming same dimensions and flow rates in both parts. However, as one of the main objectives of this research is to reach a general model that can be used in a wide range of operational conditions, they have been considered separately.

Table 1: Enthalpies of the species at 298.15 K and change of enthalpies of self-discharge reactions.

Species / Reactions	ΔH (kJ·mol^{-1})
V^{2+}	-226.0
V^{3+}	-259.0
VO^{2+}	-486.8
VO_2^+	-649.8
H_2O	-285.8
H^+	0
(3)	-91.2
(4)	-246.8
(6)	-220.0
(7)	-64.0

On the one hand, the expression for the temperature of the line that connects the cell with the tank without the pump, T_k^l, is:

$$v_k^l c_p \rho \frac{dT_k^l}{dt} = q_k c_p \rho \cdot (T^c - T_k^l) + u^l s_k^l \cdot (T^a - T_k^l) \,, \tag{32}$$

where v_k^l is the volume of this part of the pipe, u^l is the overall heat transfer coefficient of the pipe and s_k^l is the pipe surface of that section.

For the case of the tank temperature, its expression is:

$$v_k^t c_p \rho \frac{dT_k^t}{dt} = q_k c_p \rho \cdot (T_k^l - T_k^t) + u^t s_k^t \cdot (T^a - T_k^t) \,, \tag{33}$$

T_k^t being the temperature inside the posolyte or negolyte tank, u^t its heat transfer coefficient and s_k^t its surface. Finally, the temperature in the pipe line where the pump is located, T_k^p, can be expressed as:

$$v_k^p c_p \rho \frac{dT_k^p}{dt} = q_k c_p \rho \cdot (T_k^t - T_k^p) + u^p s_k^p \cdot (T^a - T_k^p) + W_k^p \,, \tag{34}$$

where v_k^p is the pipe volume of that section, u^p is the heat transfer coefficient, which is equal to u^l as both are pipes, s_k^p is its surface and W_k^p is the heat generated by the pump, which is formulated in the hydraulic model section.

Finally, the thermal model can be expressed in the state space formulation using same notation that the one used for the electrochemical model to summarize all previous expressions:

$$\dot{\boldsymbol{T}} = \mathbf{A_T}\boldsymbol{T} + \mathbf{B_{T,+}}\boldsymbol{T} \cdot q_+ + \mathbf{B_{T,-}}\boldsymbol{T} \cdot q_- + \mathbf{B_H}\boldsymbol{x} + \mathbf{b_T} \cdot j^2 + \mathbf{c_T} \cdot T^a + \mathbf{w}^p \,, \tag{35}$$

where $\boldsymbol{T}$ is the temperature state vector defined as $\boldsymbol{T} = [T^c \quad T_+^l \quad T_+^t \quad T_+^p \quad T_-^l \quad T_-^t \quad T_-^p]^\top$, matrices $\mathbf{A_T}$, $\mathbf{B_{T,+}}$ and $\mathbf{B_{T,-}}$ are related to the inlet outlet temperature and air surrounding heat, matrix $\mathbf{B_H}$ with the change of enthalpies, vector $\mathbf{b_T}$ is related to the ohmic losses, vector $\mathbf{c_T}$ with the room temperature and $\mathbf{w}^p$ with the heat generated on the pumps.

2.4 Hydraulic model

Based on different works found in the literature that describe in detail the hydraulic part of a VRFB system, a simple model is presented that only considers the elements that present a high contribution in terms of pressure drop.

This hydrualic model, like the thermal one, uses the principle of conservation of energy. In this way, the power generated by the pumps, W^p, can be computed as the product between the pressure drop inside the system, Δp, and the electrolyte flow rate q:

$$W^p = \Delta p \cdot q \,. \tag{36}$$

It should be noted that some other heat sources, such as the friction of the moving elements of the pump with the electrolytes, are neglected.

There are three different elements that have been chosen as main contributors of pressure drop, which are the pipes, the flow frames and the electrodes. The determination of the pressure drop in each part is based on the laws of fluid mechanics. The same procedure to

the one developed in the thermal model to differentiate between positive and negative parts has been used, using a variable k to distinguish between both parts.

On the one hand, the pressure drop due to the electrolyte circulating along the hydraulic pipes, Δp_k^l, can be computed as:

$$\Delta p_k^l = f \frac{l_k^l}{d_k^l} \frac{\rho v_k^2}{2} \tag{37}$$

where f is the friction loss factor, l_k^l is the length of the hydraulic pipe line in m, d_k^l is the hydraulic diameter of the pipes in m, and v_k is the velocity of the electrolyte, which is expressed in $\mathrm{m} \cdot \mathrm{s}^{-1}$ and can be computed as:

$$v_k = \frac{q_k}{s_k^l} \tag{38}$$

q_k being the electrolyte flow rate and s_k^l the cross-section of the pipe in m^2.

The pressure drop in the flow frames follows the same law and can be defined with the same expression:

$$\Delta p_k^f = f \frac{l^f}{d^f} \frac{\rho v_k^2}{2} \tag{39}$$

where l^f is the length of the electrolyte flow frames and d^f is its hydraulic diameter, which is assumed to be the same for negolyte and posolyte parts, as the cells usually have same dimensions and materials.

Finally, the pressure drop in the electrodes is calculated using Darcy's law in porous media by:

$$\Delta p_k^e = \frac{\mu q_k K_{ck} (1-\varepsilon)^2}{d_f^2 \varepsilon^3} \frac{h^e w^e}{l^e} \tag{40}$$

where μ is the viscosity of the fluid in Pa·s, K_{ck} is the Kozeny-Carman constant and d_f is the mean diameter of the electrode fibers expressed in m.

Then, the total power supplied by the pumps to overcome the pressure drop in the system can be computed as:

$$W_k^p = \left(\frac{l_k^l}{d_k^l} \frac{\rho v_k^2}{2} + f \frac{l^f}{d^f} \frac{\rho v_k^2}{2} + \frac{\mu q_k K_{ck} (1-\varepsilon)^2}{d_f^2 \varepsilon^3} \frac{h^e w^e}{l^e} \right) q_k \tag{41}$$

2.5 Voltage model

Voltage computation is one of the most important parts, since it allows to determine the power and energy stored in the system. Moreover, it is an analog variable that in practice can be measured by means of analog or digital instruments. In this way, it stands out as one of the most used variables in the validation of any VRFB model.

Ideally, the voltage of any electrochemical system can be split in two parts, which are the ideal voltage, and some losses due to different effects called overpotentials. On the one hand, the ideal voltage only depends on the species and the chemical reaction that takes place. This ideal voltage produced only by the effect of the chemical reaction is called open circuit voltage (OCV) and can be computed by means of the Nernst equation. On the other hand, the charging or discharging current across the RFB system implies the appearance of the different overpotentials such as the activation, ohmic and concentration ones. Therefore, the total voltage of a RFB, parameterized as E, can be expressed as the sum of the OCV and the overpotentials:

$$E = E^{OCV} + \eta^a + \eta^o + \eta^c \tag{42}$$

where E^{OCV} is used in this work to represent the OCV, and η^a, η^o and η^c to define the activation, ohmic and concentration overpontials, respectively.

2.5.1 OCV formulation

The computation of the OCV for any general electrochemical system is based on the Nernst equation.

For the case of a VRFB the well-knwon general expression to compute the OCV is:

$$E^{OCV} = E^\theta + \frac{RT^c}{F} ln \left(\frac{c_2 \cdot c_5 \cdot c_{H_+^+}^2}{c_3 \cdot c_4} \right) \tag{43}$$

where E^θ is the standard reduction potential and has a theoretical value of 1.256 V according to the standard potentials of each part. On the one hand, c_4, c_5 and $c_{H_+^+}$ are the molar concentration of VO^{2+} (vanadium(IV)), VO_2^+ (vanadium(V)) and hydrogen ions in the positive half-cell. On the other hand, c_2, c_3 are the molar concentration of V^{2+} and V^{3+}, in the negative side.

Nevertheless, in most studies (43) is simplified considering only the vanadium species and neglecting the effect of the protons in the positive side, assuming that have not contribution to the equilibrium potential. However, looking at equation (2) it is necessary to consider that 2 H^+ are part of the reaction. It has been reported in the literature that if they are neglected, the E^{OCV} value can differ from the real value by 100 mV [8].

Another important effect that most of the studies neglect is the Donnan potential, which is related to an unequal distribution of ions in the membrane between different ionic solutions.

Accordingly, considering the importance of the protons and having its own electrochemical model that allows to understand its evolution over the time, in this work it has been considered to add the Donnan potential to (43) obtaining the following expression for the

OCV of a VRFB:

$$E_D^{OCV} = E^\theta + \frac{RT^c}{F} ln \left(\frac{c_2^c \cdot c_5^c \cdot \left(c_{H_+^+}^c\right)^3}{c_3^c \cdot c_4^c \cdot c_{H_-^+}^c} \right) . \quad (44)$$

Considering a stack of N cells, the OCV can be computed as the sum of each individual potential. Therefore, assuming that all cells are equal, it can be computed by multiplying (44) by N.

To analyze the influence of the protons for the computation of the OCV, a SOC-OCV profile has been obtained through simulation. The SOC has been varied from 5% to 95%, considering a total vanadium concentration of 1650 mol·m^{-3}, and initial proton concentration of 1588 and 2412 mol·m^{-3} for the negative and positive sides, respectively. These initial conditions have been selected taking into account the process to obtain the electrolytes used in the experimental setup.

To simplify this first analysis as much as possible, the evolution of the vanadium and protons concentration has been directly related to the SOC. Thus, they are calculated as follows:

$$\begin{aligned} c_2^c &= c_5^c = c_v \cdot \text{SOC} \\ c_3^c &= c_4^c = c_v \cdot (1 - \text{SOC}) \\ c_{H_+^-}^c &= c_{H_+^-}^c(0) + c_v \cdot \text{SOC}/2 \\ c_{H_+^+}^c &= c_{H_+^+}^c(0) + c_v \cdot \text{SOC}/2 \ . \end{aligned}$$

Assuming a constant temperature T^c of 298 K, it is possible to compute the SOC-OCV profile of the general and most used expression (43), the same one without considering the protons, denoted as E_s^{OCV} and the ones considering the Donnan effect presented in (44).

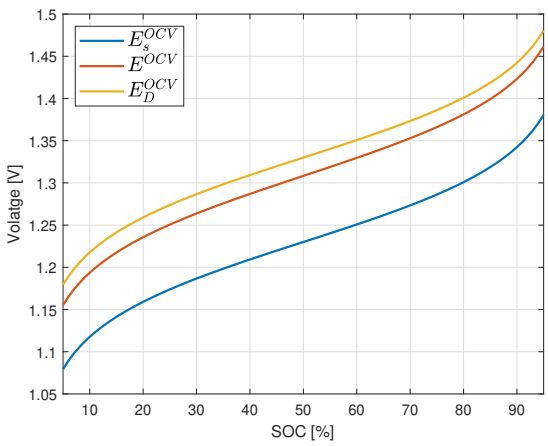

Figure 4: SOC-OCV profiles of a VRFB. E_s^{OCV}: considering only the vanadium species, E^{OCV}: considering the H protons of the posolyte and E^{OCV}: considering the Donnan effect.

Figure 4 shows the three different profiles of the OCV in terms of the SOC, where it is possible to see how there exist a large difference when the protons are not considered, and a small one considering the Donnan effect. Therefore, it can be concluded that the incorporation of protons in the VRFB model is a necessary condition for the analysis of the OCV evolution, which is one of the most important variables to be considered.

2.5.2 Activation overpotential

The activation overpotential, η^a, is defined as the potential difference required to overcome the activation energy of the redox reaction to produce a specified current. It can be computed by means of the Butler-Volmer equation, which has the following expression:

$$j_k = j_k^0 \left(e^{\frac{(1-\alpha_k)NF\eta_k^a}{RT^c}} - e^{-\frac{\alpha_k NF\eta_k^a}{RT^c}} \right) \quad (45)$$

where k is used to distinguish between the positive and negative part, j^0 is the exchange current density in A·m^{-2} and α is the charge transfer coefficient. It is important to notice, that the current density has different sign in the negative and positive parts, so $j_+ = j$ on the positive side, while $j_- = -j$ on the negative one.

Therefore, it is possible to calculate the value of the activation overpotential of a cell as:

$$\eta^a = \eta_+^a - \eta_-^a \ . \quad (46)$$

The main problem of the Butler-Volmer expression (45) is that there is not an analytical solution to obtain η^a in terms of the current density. For this reason, most of the studies use other tools to compute its value as a lookup table (LUT) or a function approximation. In this work, we present a hyperbolic sine approximation that is formulated as:

$$\eta^a = \begin{cases} \frac{RT^c}{\alpha F} \cdot sinh^{-1}\left(\frac{r_j}{2}\right) & r_j \leq \underline{b_r} \\ 0 & \underline{b_r} < r_j < \overline{b_r} \\ \frac{RT^c}{(1-\alpha)F} \cdot sinh^{-1}\left(\frac{r_j}{2}\right) & \overline{b_r} \leq r_j \end{cases} \quad (47)$$

where r_j is the ratio j/j^0 and $\underline{b_r}$ and $\overline{b_r}$ are the upper and lower bounds, respectively.

2.5.3 Ohmic overpotential

The ohmic overpotential is directly related to the cell resistance, due to the different materials used, and with the current density j.

The cell resistance can be computed as the sum of that imposed by three elements: current collectors,

membranes and electrodes. However, in some studies it has been shown that its value can vary over time and that depends on whether the system is on a charging or discharging process. In this work, its value has been considered constant differentiating between a charging or a discharging process, according to some results observed in different studies [12].

Therefore, the ohmic overpotential η^o can be computed as:

$$\eta^o = \begin{cases} r_d \cdot j & j < 0 \\ r_c \cdot j & j > 0 \end{cases} \tag{48}$$

where r_d and r_c represent the cell resistance expressed in $\Omega{\cdot}\mathrm{m}^2$.

2.5.4 Concentration overpotential

The concentration overpotential η^c is related to a potential that appears inside each electrode, due to the fact that there exist a difference between the concentration of species in the bulk electrolyte, compared to the one on the surface. This difference of concentrations in the same electrode occurs if the redox reaction of the cell is much faster than the mass transport. In this scenario, the redox reaction does not occur ideally, considering all possible species. On the one hand, it is possible that some of the reactant species do not reach the reaction, resulting in a depletion of these species. On the other hand, considering the product species, a low mass can cause that these molecules cannot be released from the reaction, resulting in an accumulation in the surface.

It is important to notice, that this phenomenon must be considered if the model presents mass transport phenomena, as diffusion, migration or convection, which actually occur in VRFB's. Accordingly, most works that consider the voltage, do not include the concentration overpotential η^c, assuming that there is not mass transfer effect and therefore, concentrations on the electrode surface do not differ from the bulk ones.

Similarly to the formulation of the activation overpotential, it is possible to calculate η^c as:

$$\eta^c = \eta^c_+ - \eta^c_- \tag{49}$$

where η^c_- and η^c_+ are the concentration overpotentials in the negative and positive half-cells, being calculated by the equations (50) and (51), respectively.

$$\eta^c_- = \frac{RT^c}{F} ln \left(\frac{1 - \dfrac{\Delta c}{c^c_3}}{1 + \dfrac{\Delta c}{c^c_2}} \right) \tag{50}$$

$$\eta^c_+ = \frac{RT^c}{F} ln \left(\frac{1 + \dfrac{\Delta c}{c^c_5}}{1 - \dfrac{\Delta c}{c^c_4}} \right) . \tag{51}$$

As can be seen, all overpotentials depend on the current, as well as on the species concentration. In order to analyze their behaviour, they have been computed numerically considering 3 different charging currents. Figure 5 presents the profiles of each one of the overpotentials in terms of SOC and current. It is possible to see how in the areas close to the maximum charge and discharge, both activation and concentration overpotentials have a large contribution in the cell voltage. Finally, Figure 6 presents the voltage profiles for the case of a charging process with a constant current of 0.9 A, comparing the OCV with and without the consideration of the Donnan effect and the overpotentials.

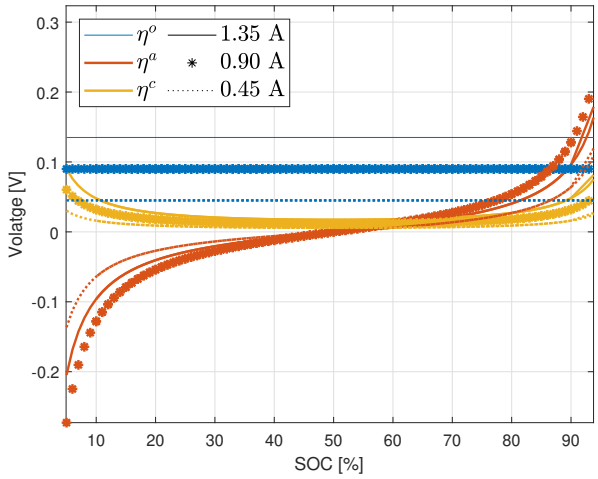

Figure 5: Overpotentials profiles of a VRFB for different values of charging current. η^o: ohmic overpotential, η^a: activation overpotential and η^c: concentration overpotential.

3 VRFB CONSERVATION LAWS

One of the main characteristics of the electrochemical model presented here, is that has been formulated according to the mass and charge conservation principles.

Under these conditions, assuming that the system is perfectly isolated and has no losses, the total amount of species will remain constant. The analysis of the mass and charge conservation can be performed using the state-space formulation.

3.1 Mass conservation

Conservation of species in terms of moles for any chemical reaction derives from the mass conservation law. Thus, it is possible to express the total number of moles of a specific species as:

$$m^k_i = c^k_i \cdot v^k \, , \tag{52}$$

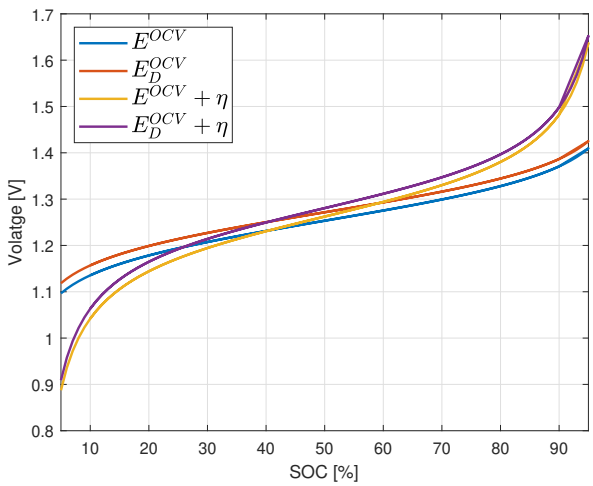

Figure 6: SOC-OCV profiles of a VRFB with and without the consideration of the Donnan effect and the overpotentials.

where m is used to express the mass, defined as the number of moles, and the superscript k represents the place that the species i occupies.

With this notation, it is possible to compute the total number of moles of any RFB, by the following expression:

$$m_t = \sum_{k=c,t} \sum_{i=2}^{5} c_i^k \cdot v^k \,, \tag{53}$$

Therefore, for the VRFB, the mass dynamics for the vanadium electrochemical model can be defined as:

$$\dot{m}_t = \boldsymbol{v} \cdot \dot{\boldsymbol{x}} \,, \tag{54}$$

where $\dot{m}_t$ defines the dynamics of the number of moles along the time, thus having units of mol·s^{-1} and $\boldsymbol{v}$ is the volume vector of a RFB defined as $\boldsymbol{v}$=$[v^c \;\; v^c \;\; v^c \;\; v^c \;\; v_-^t \;\; v_-^t \;\; v_+^t \;\; v_+^t]$.

Finally, substituting (15) in the previous expression, it is obtained:

$$\dot{m}_t = \boldsymbol{v} \cdot (\mathbf{A}\boldsymbol{x} + \mathbf{B}_-\boldsymbol{x} \cdot q_- + \mathbf{B}_+\boldsymbol{x} \cdot q_+ + \mathbf{b} \cdot j) = 0 \,, \tag{55}$$

which indicates that the mass conservation law is fulfilled for the vanadium electrochemical model.

Although (55) shows that the total mass is preserved in the global system it does not give information about the behaviour in each half-cell. In this work, the diffusion mechanism has been chosen as an ion crossover effect. Therefore, it is possible to see how the mass changes in each part of the battery due to this effect.

For the case of the negative side, the mass conservation study can be performed with the negolyte volume vector $\boldsymbol{v}_-$, defined as $\boldsymbol{v}_-$=$[v^c \;\; v^c \;\; 0 \;\; 0 \;\; v_-^t \;\; v_-^t \;\; 0 \;\; 0]$. In this way, it is possible to obtain the following expression:

$$\dot{m}_- = \boldsymbol{v}_- \cdot \mathbf{A}\boldsymbol{x} = \frac{s^m}{w^m} \cdot \left(-k_2 c_2^c - k_3 c_3^c + k_4 c_4^c + k_5 c_5^c\right) . \tag{56}$$

On the other hand, considering the posolyte side, computing the mass differential equation with the volume vector $\boldsymbol{v}_+$=$[0 \;\; 0 \;\; v^c \;\; v^c \;\; 0 \;\; 0 \;\; v_+^t \;\; v_+^t]$, the same results can be extrapolated with opposite sign:

$$\dot{m}_+ = \boldsymbol{v}_+ \cdot \mathbf{A}\boldsymbol{x} = \frac{s^m}{w^m} \cdot \left(k_2 c_2^c + k_3 c_3^c - k_4 c_4^c - k_5 c_5^c\right) . \tag{57}$$

From the expressions presented in (56) and (57) it is possible to see how the sum of both makes the total mass equal to zero, so the mass is conserved in the entire system. However, it can be seen how the mass will be different in each part if the species concentration and the diffusion coefficients are not equal.

The initial species concentration can be known when the electrolytes are prepared. However the exact value of the diffusion coefficients is difficult to know, even more if the dependence on T^c, as expressed in (13), is considered. Due to the impossibility of being able to measure their values, there is no consensus on their values or ratios between them, although the following relationship is satisfied

$$k_2 > k_4 > k_5 > k_3. \tag{58}$$

Using this relationship, it is possible to analyze where and how fast the species are moving through the membrane. In order to compute it, a real Nafion membrane with a thickness of 125 μm, has been considered. Table 2 summarizes the different diffusion coefficients. They have been computed using the Arrhenius equation (13), considering the pre-factors of the commercial membranes and a constant electrolyte temperature of 298 K. As it can be noticed, the diffusion coefficients follow the relationship presented in (58).

Table 2: Pre-factors and diffusion coefficients of the different vanadium species for a Nafion membrane [27].

Vanadium species	Pre-factor A (m^2·s^{-1})	Diffusion Coefficient k (m^2· s^{-1})
V^{2+}	$9.6 \cdot 10^{-9}$	$8.83 \cdot 10^{-12}$
V^{3+}	$3.5 \cdot 10^{-9}$	$3.22 \cdot 10^{-12}$
V^{4+}	$1.1 \cdot 10^{-8}$	$6.83 \cdot 10^{-12}$
V^{5+}	$6.4 \cdot 10^{-9}$	$5.83 \cdot 10^{-12}$

In order to analyze the diffusion mechanism, as well as checking the principle of mass conservation, some simulations have been performed. The considered RFB facility is formed by two tanks of 100 ml of capacity, and a cell with the dimensions shown in Table 3, considering a total concentration of 0.4 M.

Table 3: Model parameters for the conservation of mass study.

Parameter	Value
v_-^t	$1{\cdot}10^{-4}$ m^3
v_+^t	$1{\cdot}10^{-4}$ m^3
s^e	$9{\cdot}10^{-4}$ m^2
s^m	$9{\cdot}10^{-4}$ m^2
w^e	$5{\cdot}10^{-3}$ m

Considering these characteristics, the total mass of the system according to expression (53) is 0.004 mol. Assuming that the system is initially balanced, with same concentration of 1000 mol·m^{-3} for each vanadium species, a simulation of the diffusion phenomenon has been performed. Figure 7 shows the evolution of the four vanadium species, until the equilibrium is reached. However, it is important to remark that the transport of species due to diffusion will stop when one of them disappears, as it happens with c_2. The evolution of the system mass is shown in Figure 8 where it can be observed that the total mass m_t is constant according to the mass conservation principle with an approximate value of 0.004 moles.

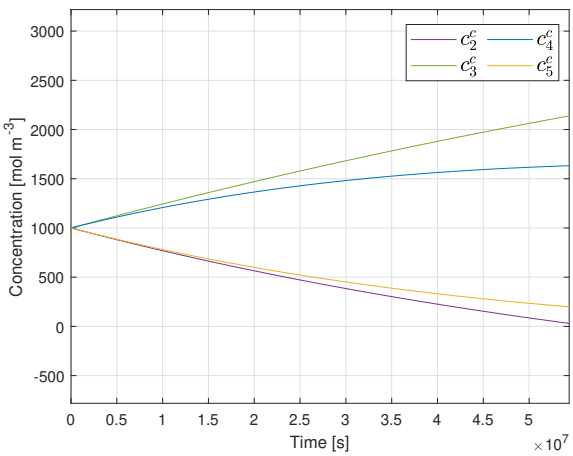

Figure 7: Evolution of vanadium species due to diffusion phenomenon.

The negolyte mass, denoted as m_-, increases with time while the posolyte one, m_+, decreases, clarifying the mass transport.

3.2 Charge conservation

Using the same procedure developed to analyze mass conservation, it is possible to evaluate if charge conservation is also fulfilled. In this case, it is important to consider that each vanadium species has its own charge which is directly related to its oxidation state. Thus, the

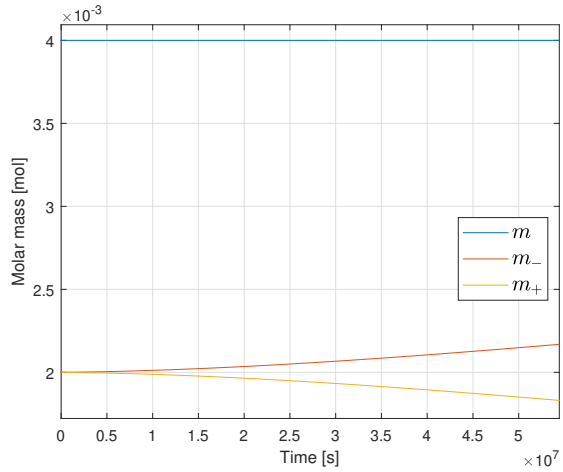

Figure 8: Evolution of total mass m, and posolyte, m_+, and negolyte m_- due to diffusion phenomenon.

expression for the total charge of the system depending on the number of moles of each species is:

$$c_t = (2c_2^c + 3c_3^c + 2c_4^c + c_5^c)v^c + (2c_2^t + 3c_3^t)v_-^t + (2c_4^t + c_5^t)v_+^t \,, \tag{59}$$

where c_t is used to express the total charge of the system, which depends on the valence i of each vanadium species V^{i+}. Similarly to the analysis performed for the total number of moles, m_t, it is possible to analyze the total charge dynamics as:

$$\dot{c}_t = \boldsymbol{v_c} \cdot \dot{\boldsymbol{x}} \,, \tag{60}$$

where the volume vector is $\boldsymbol{v_c} = [2v^c, 3v^c, 2v^c, v^c, 2v_-^t, 3v_-^t, 2v_+^t, v_+^t]$, obtaining that its value is zero, which means that the total charge remains constant inside the system:

$$\dot{c}_t = \boldsymbol{v_c} \cdot (\mathbf{A}\boldsymbol{x} + \mathbf{B}_-\boldsymbol{x} \cdot q_- + \mathbf{B}_+\boldsymbol{x} \cdot q_+ + \mathbf{b} \cdot j) = 0 \,. \tag{61}$$

4 EXPERIMENTAL VALIDATION

In order to validate the model, some different experiments have been carried out with a real VRFB cell. A discharge process to calibrate the model parameters has been considered to later develop a series of charge and discharge cycles in order to be able to see the effect of the ion crossover. The change of the mass in each side of the system, which is translated in the estimation of the SOH, has been identified.

The experimental set-up used in this work consists of a VRFB single cell developed by the Instituto de Carboquímica, two tanks and two peristaltic pumps. The cell consists of two 7x7 cm^2 porous electrodes separated by a Nafion-212 membrane. Each tank contains 80 ml

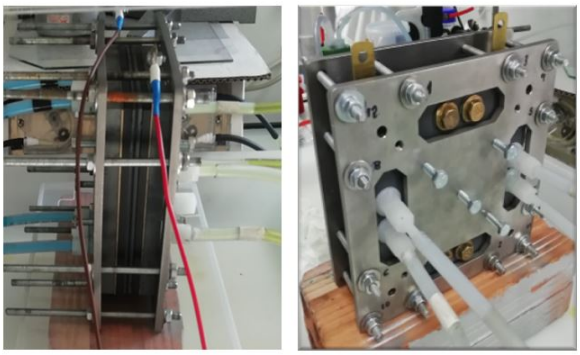

Figure 9: VRFB single cell assembled in the Instituto de Carboquímica center.

of 1.6 M vanadium solutions in 2 M sulphuric acid and 0.05 M phosphoric acid.

The first experiment performed consists of a discharge cycle at a constant current of 3 A where the voltage has been measured every 1 second, without a certain idea of the initial conditions in terms of initial species concentration.

Despite the fact that many of the variables and parameters of the system are known or can be measured, there is no information available about some others and they need to be estimated. For this purpose, the use of estimation methods is required, and an offline estimator based on the PSO technique is proposed. The parameters and variables that have been considered in this work are the initial species concentrations, and the parameters related to the different overpotentials, which are the cell resistance r and the charge transfer coefficients α_+ and α_-. For the case of the standard electrode potential E^{θ}, it is estimated considering the effect of the Donnan potential on its computation, being denoted as E^{θ^*}.

Under the assumption of high flow rates and the mass and charge conservation principles, it is possible to reduce the original system to a 1st order model, being only necessary to calibrate one of the initial concentrations, which in this case is the vanadium species c_2.

Using a PSO technique [2], it is possible to estimate the set of parameters $\mathbf{p} = [\alpha_+, \alpha_-, r_d, E^{\theta^*}, c_2(0)]$, that satisfy the following problem:

$$\begin{aligned} \min_{\mathbf{p}} \quad & \sum_{k=1}^{N} |E(k \cdot T_s) - \hat{E}(k \cdot T_s)| \\ \text{subject to} \quad & \\ & \hat{E}(k \cdot T_s) = f(\mathbf{p}) \\ & \mathbf{c}(\mathbf{p}) \leq \mathbf{0} \end{aligned}$$

N being the total number of measures that have been taken, considering an equal sample period T_s, k denotes each sample and $\mathbf{c}$ is the constraint set of the unknown parameters. For the experiment performed, the value of T_s is one second and the constraint set is $\mathbf{c}(\mathbf{p}) = [0..1, 0..1, 0..0.5, 0..2, 0..1600]$.

Table 4: Measured and calibrated VRFB parameters.

Nomenclature	Value	Obtanining
c_t	0.896 mol e$^-$	Measured
m_t	0.264 mol	Measured
m_+	0.132 mol	Measured
T	298 K	Measured
v^c	$7.5{\cdot}10^{-6}$ m^3	Measured
v^t_-	$8{\cdot}10^{-5}$ m^3	Measured
v^t_+	$8{\cdot}10^{-5}$ m^3	Measured
α_+	0.51	Estimated
α_-	0.495	Estimated
$c_2(0)$	1457 mol·m^{-3}	Estimated
E^{θ^*}	1.235 V	Estimated
r_d	0.11 Ω	Estimated

Figure 10 shows the profile of the actual voltage E measured during the discharging profile at constant current, and the estimated ones with the calibrated parameters depicted in Table 4. As can be noticed, the agreement is reasonably good, presenting a similar voltage performance along all the discharging profile.

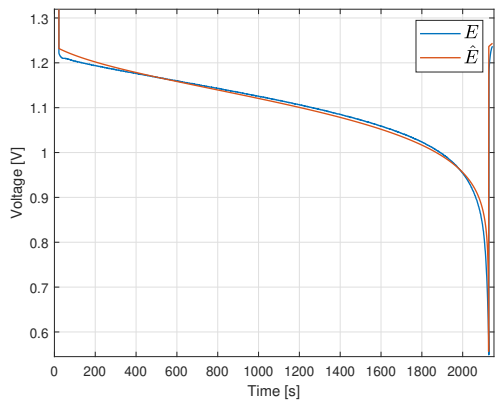

Figure 10: Measured voltage and the estimated ones with the model calibrated.

In order to determine if the model presented is able to be used in long-term scenarios when the ion crossover effect is present inside the battery, a series of charge and discharge processes have been carried out. Using the calibrated model and assuming that there is not ion crossover phenomena and that the mass in both sides remains constant and equal to 0.132 mol, the profile obtained is the one shown in Figure 11.

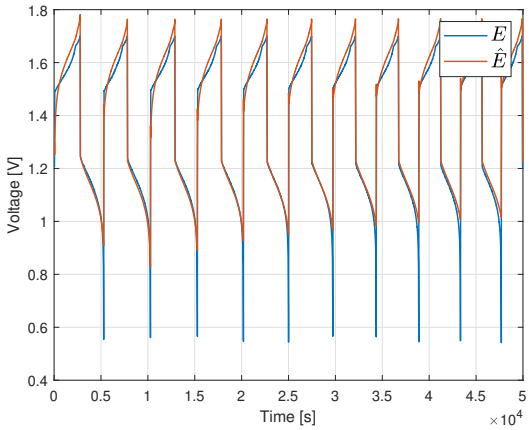

Figure 11: Measured voltage and the estimated ones assuming not change of mass in each side.

As can be noticed, there exists a difference between the measured voltage and the one obtained from the model. It is also possible to see the effect of the ion crossover. This experiment consists in charging the system with a constant current until it reaches a maximum voltage value, and discharging it until a minimum one. As can be observed, initially the duration of the cycles is approximately 5000 seconds, while at the end of the profile, it is reduced to around 4300 seconds.

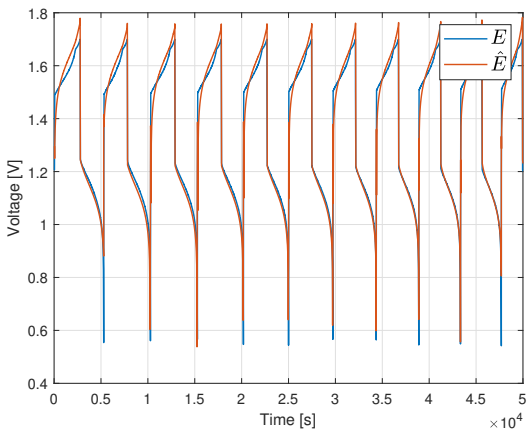

Figure 12: Measured voltage and the estimated ones with a variable m_+.

The difficulty of estimating low vanadium concentrations in addition to the existence of side reactions influences especially in the high voltage region during charging. This voltage model, based on the Nernst equation, is highly sensitive to small variations in vanadium concentration when the SOC is very high or very low, so it is necessary to improve the concentration estimation.

In order to minimize the error in vanadium concentration, in the implementation of the model with this experiment, it has been considered that the mass in the posolyte changes as a ramp, calibrating the value of the slope in order to estimate the change of mass, and therefore, the SOH. Performing this analysis using the same PSO algorithm developed previously and introducing this new parameter for the estimation, the results obtained are the ones shown in Figure 12.

In this case the agreement of the voltage is reasonably good compared to the previous ones that did not consider the mass variation due to crossover. The maximum relative errors, reached at high voltage during the charging process, are greater than 50% without considering mass transport but below 20% in most cycles when mass transport is considered. The very high deviation observed during the short period of time that the system is above 1.7 V may be related, in addition to the difficulty of estimating low vanadium concentrations, to the existence of side reactions. Nevertheless, the mean relative error of the estimation considering mass transport is around 1.7%. Therefore, and assuming that the system was initially balanced, it is possible to obtain the profile of the variation of the SOH which is presented in Figure 13.

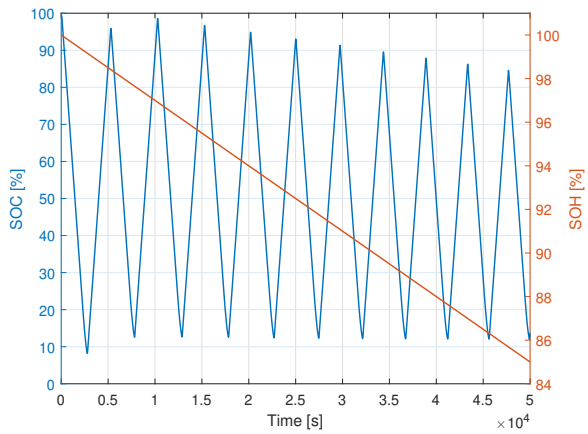

Figure 13: SOC and SOH obtained from the model calibrated considering a variable m_+.

5 Conclusion

This work presents a new dynamic model of a VRFB that allows to consider the most important variables and effects that occur during the operation of the system. The calibration performed with the PSO technique achieved very accurate results with the data obtained from a discharge experiment, validating the presented model that considers different variables. The correctness of the model is guaranteed not only for SOC es-

timation, but it is also able to estimate the SOH when the effect of the ion transport mechanisms is present in a real vanadium redox flow battery. As future improvements, it would be necessary to analyze the robustness of the model presented for the case of a stack where the bypass currents can have an important effect.

Acknowledgements

This research has been developed within the CSIC Interdisciplinary Thematic Platform (PTI+) Transición Energética Sostenible+ (PTI-TRANSENER+) as part of the CSIC program for the Spanish Recovery, Transformation and Resilience Plan funded by the Recovery and Resilience Facility of the European Union, established by the Regulation (EU) 2020/2094, the Spanish Ministry of Science and Innovation under projects MAFALDA (PID2021-126001OB-C31 and C32 funded by MCIN/AEI/ 10.13039/501100011033 / ERDF, EU), and MASHED (TED2021-129927B-I00), and by the Spanish Ministry of Universities funded by the European Union - NextGenerationEU (2022UPC-MSC-93823).

References

[1] Badrinarayanan, R., Zhao, J., Tseng, K., Skyllas-Kazacos, M.: Extended dynamic model for ion diffusion in all-vanadium redox flow battery including the effects of temperature and bulk electrolyte transfer. Journal of Power Sources **270**, 576 – 586 (2014), doi:10.1016/j.jpowsour.2014.07.128

[2] Clemente, A., Montiel, M., Barreras, F., Lozano, A., Costa-Castelló, R.: Vanadium redox flow battery state of charge estimationusing a concentration model and a sliding mode observer. IEEE Access **9**, 72368–72376 (2021), doi:10.1109/ACCESS.2021.3079382

[3] Clemente, A., Costa-Castelló, R.: Redox flow batteries: A literature review oriented to automatic control. Energies **13**, 4514 (09 2020), doi:10.3390/en13174514

[4] Doetsch, C., Pohlig, A.: 13 - the use of flow batteries in storing electricity for national grids. In: Letcher, T.M. (ed.) Future Energy (Third Edition), pp. 263–277. Elsevier, third edition edn. (2020), doi:10.1016/B978-0-08-102886-5.00013-X

[5] Gu, F.C., Chen, H.C., Li, K.Y.: Mathematic modeling and performance analysis of vanadium redox flow battery. Energy & Fuels **34**(8), 10142–10147 (2020), doi:10.1021/acs.energyfuels.0c01536

[6] Khaki, B., Das, P.: Fast and simplified algorithms for soc and soh estimation of vanadium redox flow batteries. In: 2021 IEEE Green Technologies Conference (GreenTech). pp. 494–501 (2021), doi:10.1109/GreenTech48523.2021.00083

[7] Knehr, K., Kumbur, E.: Open circuit voltage of vanadium redox flow batteries: Discrepancy between models and experiments. Electrochemistry Communications **13**(4), 342–345 (2011), doi:10.1016/j.elecom.2011.01.020

[8] Knehr, K., Kumbur, E.: Open circuit voltage of vanadium redox flow batteries: Discrepancy between models and experiments. Electrochemistry Communications **13**(4), 342–345 (2011), doi:10.1016/j.elecom.2011.01.020

[9] Langner, J., Melke, J., Ehrenberg, H., Roth, C.: Determination of overpotentials in all vanadium redox flow batteries. ECS Transactions **58**(37), 1 (apr 2014), doi:10.1149/05837.0001ecst

[10] Lei, Y., Zhang, B., Bai, B., Zhao, T.: A transient electrochemical model incorporating the donnan effect for all-vanadium redox flow batteries. Journal of Power Sources **299**, 202–211 (2015), doi:10.1016/j.jpowsour.2015.08.100

[11] Li, Y., Sun, L., Cao, L., Bao, J., Skyllas-Kazacos, M.: Dynamic model based membrane permeability estimation for online soc imbalances monitoring of vanadium redox flow batteries. Journal of Energy Storage **39** (7 2021), doi:10.1016/j.est.2021.102688

[12] Mazur, P., Mrlik, J., Charvat, J., Pocedic, J., Vrana, J., Dundalek, J., Kosek, J.: A complex four-point method for the evaluation of ohmic and faradaic losses within a redox flow battery single-cell. MethodsX **6**, 534–539 (2019), doi:10.1016/j.mex.2019.03.007

[13] Murthy, S.K., Sharma, A.K., Choo, C., Birgersson, E.: Analysis of concentration overpotential in an all-vanadium redox flow battery. Journal of The Electrochemical Society **165**(9), A1746 (jun 2018), doi:10.1149/2.0681809jes

[14] Nolte, O., Volodin, I.A., Stolze, C., Hager, M.D., Schubert, U.S.: Trust is good, control is better: A review on monitoring and characterization techniques for flow battery electrolytes. Materials Horizons **8**, 1866–1925 (7 2021), doi:10.1039/d0mh01632b

[15] Oh, K., Moazzam, M., Gwak, G., Ju, H.: Water crossover phenomena in all-vanadium redox flow batteries. Electrochimica Acta **297**, 101–111 (2019), doi:10.1016/j.electacta.2018.11.151

[16] Oh, K., Won, S., Ju, H.: A comparative study of species migration and diffusion mechanisms in all-vanadium redox flow batteries. Electrochimica Acta **181**, 238–247 (2015), doi:/10.1016/j.electacta.2015.03.012

[17] Puleston, T., Clemente, A., Costa-Castelló, R., Serra, M.: Modelling and estimation of vanadium redox flow batteries: A review. Batteries **8**(9) (2022), doi:10.3390/batteries8090121

[18] Skyllas-Kazacos, M., Goh, L.: Modeling of vanadium ion diffusion across the ion exchange membrane in the vanadium redox battery. Journal of Membrane Science **399-400**, 43–48 (2012), doi:10.1016/j.memsci.2012.01.024

[19] Skyllas-Kazacos, M., Menictas, C.: Vanadium redox flow batteries. In: Cabeza, L.F. (ed.) Encyclopedia of Energy Storage, pp. 407–422. Elsevier, Oxford (2022), doi:10.1016/B978-0-12-819723-3.00050-0

[20] Tang, A., Bao, J., Skyllas-Kazacos, M.: Thermal modelling of battery configuration and self-discharge reactions in vanadium redox flow battery. Journal of Power Sources **216**, 489–501 (2012), doi:10.1016/j.jpowsour.2012.06.052

[21] Tang, A., Bao, J., Skyllas-Kazacos, M.: Thermal modelling of battery configuration and self-discharge reactions in vanadium redox flow battery. Journal of Power Sources **216**, 489–501 (10 2012), doi:10.1016/j.jpowsour.2012.06.052

[22] Tang, A., Bao, J., Skyllas-Kazacos, M.: Studies on pressure losses and flow rate optimization in vanadium redox flow battery. Journal of Power Sources **248**, 154–162 (2014), doi:10.1016/j.jpowsour.2013.09.071

[23] Tang, A., McCann, J., Bao, J., Skyllas-Kazacos, M.: Investigation of the effect of shunt current on battery efficiency and stack temperature in vanadium redox flow battery. Journal of Power Sources **242**, 349–356 (2013), doi:10.1016/j.jpowsour.2013.05.079

[24] Tang, A., Ting, S., Bao, J., Skyllas-Kazacos, M.: Thermal modelling and simulation of the all-vanadium redox flow battery. Journal of Power Sources **203**, 165–176 (2012), doi:10.1016/j.jpowsour.2011.11.079

[25] Trovò, A., Saccardo, A., Giomo, M., Guarnieri, M.: Thermal modeling of industrial-scale vanadium redox flow batteries in high-current operations. Journal of Power Sources **424**, 204–214 (2019), doi:10.1016/j.jpowsour.2019.03.080

[26] Xing, Y., Bernadet, L., Torrell, M., Tarancón, A., Costa-Castelló, R., Na, J.: Offline and online parameter estimation of nonlinear systems: Application to a solid oxide fuel cell system. ISA Transactions (2022), doi:10.1016/j.isatra.2022.07.025

[27] Yan, Y., Skyllas-Kazacos, M., Bao, J.: Effects of battery design, environmental temperature and electrolyte flowrate on thermal behaviour of a vanadium redox flow battery in different applications. Journal of Energy Storage **11**, 104–118 (2017), doi:10.1016/j.est.2017.01.007